

Ptychographic wavefront characterization for single-particle imaging at x-ray lasers: supplement

BENEDIKT J. DAURER,^{1,2,3}  SIMONE SALA,^{3,4,5}  MAX F. HANTKE,⁶ HEMANTH K. N. REDDY,² JOHAN BIELECKI,^{2,7} ZHOU SHEN,^{1,8} CARL NETTELBLAD,^{2,9}  MARTIN SVENDA,^{2,10} TOMAS EKEBERG,² GABRIELLA A. CARINI,^{11,12} PHILIP HART,¹¹ TIMUR OSIPOV,¹¹ ANDREW AQUILA,¹¹ N. DUANE LOH,^{1,8,*} FILIPE R. N. C. MAIA,^{2,13} AND PIERRE THIBAUT^{3,5,14}

¹Centre for BioImaging Sciences, National University of Singapore, Singapore 117557, Singapore

²Laboratory of Molecular Biophysics, Department of Cell and Molecular Biology, Uppsala University, SE-75124 Uppsala, Sweden

³Diamond Light Source, Harwell Science & Innovation Campus, Didcot OX11 0DE, UK

⁴Department of Physics & Astronomy, University College London, London WC1E 6BT, UK

⁵Department of Physics & Astronomy, University of Southampton, Southampton SO17 1BJ, UK

⁶Physical and Theoretical Chemistry Laboratory, Oxford University, Oxford OX1 3QZO, UK

⁷European XFEL GmbH, Holzkoppel 4, 22869 Schenefeld, Germany

⁸Department of Physics, National University of Singapore, Singapore 117557, Singapore

⁹Division of Scientific Computing, Department of Information Technology, Science for Life Laboratory, Uppsala University, SE-75105 Uppsala, Sweden

¹⁰Department of Applied Physics, Biomedical and X-Ray Physics, KTH—Royal Institute of Technology, SE 10691 Stockholm, Sweden

¹¹SLAC National Accelerator Laboratory, 2575 Sand Hill Road, Menlo Park, California 94025, USA

¹²Brookhaven National Laboratory, Upton, New York 11973, USA

¹³NERSC, Lawrence Berkeley National Laboratory, Berkeley, California 94720, USA

¹⁴Università degli Studi di Trieste, Trieste 34127, Italy

*Corresponding author: duaneloh@nus.edu.sg

This supplement published with The Optical Society on 12 April 2021 by The Authors under the terms of the [Creative Commons Attribution 4.0 License](https://creativecommons.org/licenses/by/4.0/) in the format provided by the authors and unedited. Further distribution of this work must maintain attribution to the author(s) and the published article's title, journal citation, and DOI.

Supplement DOI: <https://doi.org/10.6084/m9.figshare.14192756>

Parent Article DOI: <https://doi.org/10.1364/OPTICA.416655>

Ptychographic wavefront characterisation for single-particle imaging at X-ray lasers: supplemental document

1. ESTIMATING THE TRANSMISSION THROUGH THE OPTICAL SYSTEM AT THE AMO ENDSTATION

In the same setup as the ptychographic experiment described in this article, we also collected 18.5k single-shot intensity images of the direct beam passing only through the 110 nm thick support membrane of the test target and recorded on the back pnCCD. A few examples are shown in

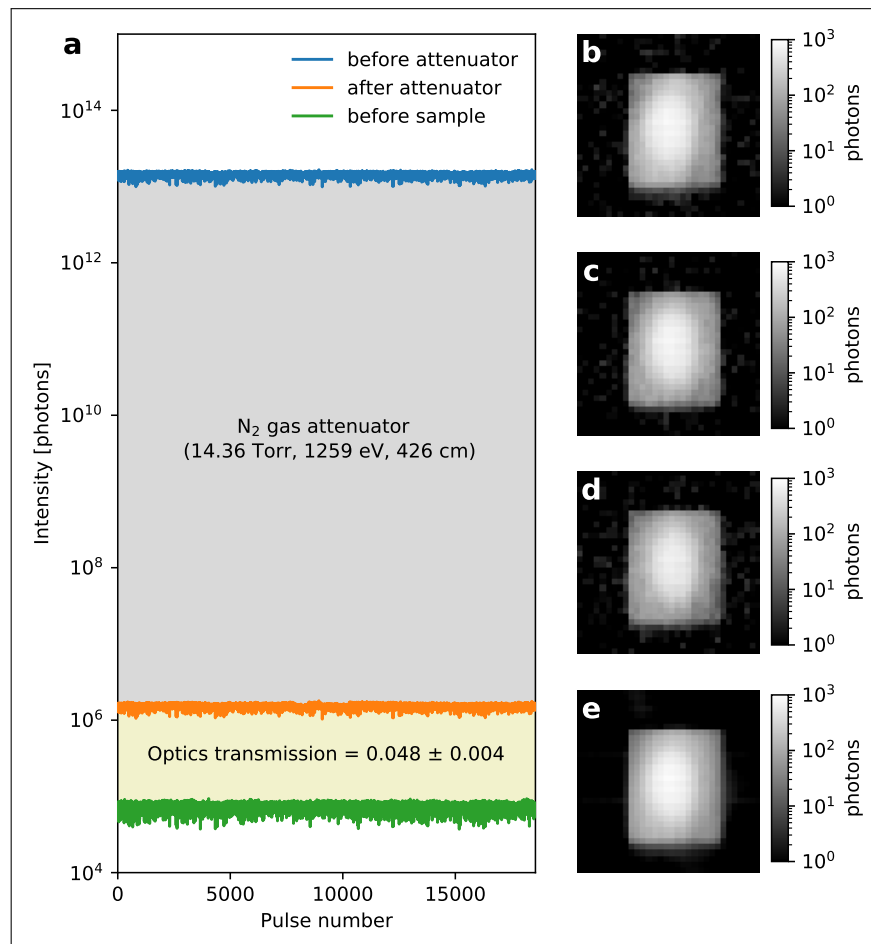


Fig. S1. Calibration measurement with attenuated beam through Si_3N_4 membrane. (a) Full beam intensity measured for each pulse before the attenuator (blue) and after the attenuator (orange) based on expected transmission through 426 cm of N_2 gas. Intensity measured for each pulse on the pnCCD corrected for transmission through 110 nm of Si_3N_4 and $0.3 \mu\text{m}$ of polyimide shielding (green). (b-d) Examples of single-shot intensity measurements on the pnCCD. (e) Average over all single-shot measurements.

Fig. S1b-d with the intensity pattern averaged over all events shown in Fig. S1e. We can use these direct measurements of the attenuated AMO beam to estimate the transmission through the beamline. For each image, we converted the analogue-to-digital (ADU) signal to photons (6.15 ADUs per photon at 1259 eV and gain mode 1) and integrated the signal over all pixels. The integrated intensity was corrected for transmission through a 0.3 μm thick polyimide filter (placed in front of the pnCCD to protect the detector chips) and 110 nm of Si_3N_4 , which consequently estimates the intensity before the sample plane (green trace in Fig. S1a).

The recorded full beam intensity, measured by a gas monitor just upstream of the attenuator, was about (2.92 ± 0.15) mJ on average (equivalent to 1.45×10^{13} photons) and is shown as a blue trace in Fig. S1a. Because we were using the gas attenuator to reduce the intensity of the beam by 7 orders of magnitude, we could not use the downstream gas monitors to directly measure the attenuated intensity. But we can calculate the transmission through the N_2 gas cell via the Henke tables [1], assuming a length of 426 cm (aperture-to-aperture based on technical drawing), a temperature of 25 $^\circ\text{C}$ [2] and using the given values for gas pressure and photon energy recorded in each shot. With this, we can estimate the reduced intensity just after the gas attenuator (orange trace in Fig. S1a). By comparing the given intensities, we can then estimate the transmission through all the optical components of the beamline at 4.8% on average with a standard deviation of 0.4% based on shot-to-shot variations.

2. FOURIER ANALYSIS OF POSITIONAL VARIATIONS

Figure S2 summarises the positional variation found during the ptychographical experiment at the AMO endstation, comparing data that was collected with the cooling head of the pnCCD being turned on and off, and indicating the most prominent frequencies present, see Fig. S2d.

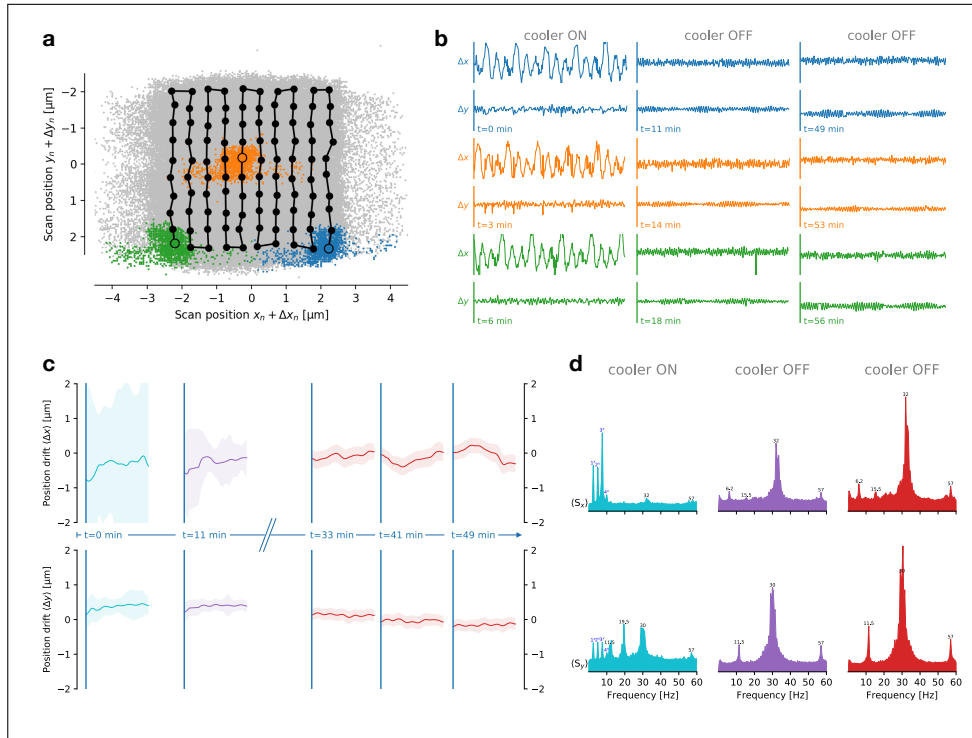


Fig. S2. (a) Overview of the scan position for a total of 5 data sets, black circles indicate the original positions, gray dots indicate the updated ones. For the first data set, the pnCCD cooler was on, while it was turned off for all other data sets. (b) Variation around 3 different scan positions for 240 consecutive pulses separately shown for data recorded at 3 different time points. The vertical bars have a length of 4 μm . (c) Average variation around all original scan positions shown separately for all 5 data sets. The shaded area indicates ± 1 standard deviation. (d) Fourier analysis of the positional variation with most prominent frequencies being indicated by black numbers. The blue numbers indicate multiples of 2.5 Hz.

3. CORRELATION OF SINGLE-PULSE VARIATIONS WITH UPSTREAM ELECTRON AND PHOTON BEAM PARAMETERS

For each of the 90k pulses used in this ptychographic experiment, we have extracted the so called EBEAM parameters, a set of quantities that measure properties of the electron and photon beam along their trajectory in the accelerator tunnel and inside the optics hutches. A good explanation for most of these parameters can be found in [3]. We correlated these EBEAM parameters with the variations in position ($\Delta x, \Delta y$), phase tilt ($\alpha_x, \alpha_y, \beta_x, \beta_y$) and incoherent mode coefficients ($c_0 - c_4$) that we found during the single-pulse fitting step of our reconstruction pipeline (Table S1). For this purpose, we have chosen the Spearman's rank correlation as a robust non-parametric metric testing the monotonicity of the relationship between two datasets.

Table S1. Spearman's rank correlation between a set of downstream single-pulse measurements (position shifts, phase tilts, coefficients associated with the 5 probe modes) and upstream electron and photon beam diagnostic (EBEAM) parameters. GMD is the gas monitor detector which tracks the fluence for each pulse. Positive correlation above 50% is shown in blue, negative correlation above 50% is shown in red, and all other correlations are shown in gray.

Parameters	Δx	Δy	α_x	α_y	β_x	β_y	c_0	c_1	c_2	c_3	c_4
Charge	-0.1	0.1	0.0	-0.1	0.0	-0.1	0.1	0.2	0.1	0.1	0.0
DumpCharge	-0.1	0.1	0.2	-0.1	0.1	-0.1	0.0	0.1	-0.1	0.0	-0.1
EnergyBC1	0.1	0.0	-0.2	0.0	-0.1	0.1	0.2	0.1	0.2	0.1	0.1
EnergyBC2	-0.1	0.0	0.7	-0.1	0.3	-0.2	-0.5	-0.3	-0.7	-0.4	-0.2
L3Energy	0.1	0.0	-0.8	0.1	-0.3	0.3	0.6	0.3	0.8	0.4	0.3
LTU250	0.1	0.0	-0.8	0.1	-0.3	0.3	0.6	0.3	0.8	0.4	0.3
LTU450	-0.1	0.0	0.8	-0.1	0.3	-0.3	-0.6	-0.3	-0.8	-0.4	-0.3
LTUAngX	-0.1	0.0	0.8	0.0	0.4	-0.3	-0.5	-0.2	-0.8	-0.3	-0.3
LTUAngY	0.2	0.1	-0.8	-0.1	-0.5	0.2	0.5	0.3	0.7	0.2	0.1
LTUPosX	0.1	0.0	0.3	0.1	0.0	-0.2	-0.2	0.1	-0.4	-0.2	-0.3
LTUPosY	0.2	0.0	-0.8	0.0	-0.4	0.3	0.5	0.2	0.8	0.3	0.2
PhotonEnergy	0.1	0.0	-0.8	0.1	-0.3	0.3	0.6	0.3	0.8	0.4	0.3
PkCurrBC1	0.0	0.0	0.0	-0.1	0.0	0.0	0.1	0.0	0.1	0.1	0.0
PkCurrBC2	0.0	0.0	0.0	-0.1	0.0	0.0	0.1	0.0	0.1	0.1	0.0
UndAngX	0.0	0.0	-0.5	0.1	-0.1	0.3	0.2	0.1	0.6	0.3	0.3
UndAngY	0.1	0.0	-0.1	-0.7	-0.1	0.1	0.1	-0.3	0.0	-0.1	0.0
UndPosX	0.0	0.0	0.0	0.0	0.0	0.0	0.0	0.0	0.0	0.0	0.0
UndPosY	0.1	0.0	-0.6	0.4	-0.3	0.3	0.3	0.4	0.6	0.4	0.1
GMD	0.0	0.0	-0.1	0.3	-0.1	0.0	0.6	0.3	0.0	0.2	0.2

4. CONVERSION FROM PHASE TILTS TO TRANSLATIONS OF DIFFRACTION PATTERNS

The wavefront of an XFEL pulse, of wavevector $k = 2\pi/\lambda$ propagating mostly along the \hat{z} optical axis, near the focus (\vec{r}_0) at position $\vec{r}_0 + \Delta\vec{r}$ can be written as

$$\begin{aligned} \psi(\vec{r}) &= M(\vec{r}) \exp[i\alpha(\vec{r})] \\ &\approx M(\vec{r}) \exp\left[i\left[\alpha(\vec{r}_0) + \vec{\nabla}\alpha|_{\vec{r}_0} \cdot \Delta\vec{r}\right]\right], \end{aligned} \quad (\text{S1})$$

where $M(\vec{r})$ is a real-valued function, and the gradient term in the phase is approximated here as based on our reconstructed wavefront at \vec{r}_0

$$\begin{aligned}\vec{\nabla}\alpha|_{\vec{r}_0} &= \frac{\partial\alpha}{\partial z}\Big|_{\vec{r}_0}\hat{z} + \frac{\partial\alpha}{\partial x}\Big|_{\vec{r}_0}\hat{x} + \frac{\partial\alpha}{\partial y}\Big|_{\vec{r}_0}\hat{y} \\ &\approx k'\hat{z} + \frac{\alpha_x}{\delta}\hat{x} + \frac{\alpha_y}{\delta}\hat{y},\end{aligned}\quad (\text{S2})$$

with $k' = \sqrt{k^2 - (\alpha_x/\delta)^2 - (\alpha_y/\delta)^2}$ to conserve energy during ‘free-wave’ propagation in vacuum, and δ defined as the pixel size of the reconstructed wavefront near the focus. The unit vector

$$\Delta\vec{r} = \frac{1}{k}\left(k'\hat{z} + \frac{\alpha_x}{\delta}\hat{x} + \frac{\alpha_y}{\delta}\hat{y}\right), \quad (\text{S3})$$

which is pointed in the direction parallel to $\vec{\nabla}\alpha|_{\vec{r}_0}$, now defines the first order phase tilt. Hence, the angular offsets (θ_x, θ_y) of the center of the Fraunhofer diffraction of $\psi(\vec{r}_0)$ due to this phase tilt is

$$\theta_x = \frac{\alpha_x}{\delta k'} \approx \frac{\alpha_x}{\delta k} = \frac{\alpha_x \lambda}{2\pi\delta} \quad (\text{S4})$$

$$\theta_y = \frac{\alpha_y}{\delta k'} \approx \frac{\alpha_y}{\delta k} = \frac{\alpha_y \lambda}{2\pi\delta}. \quad (\text{S5})$$

5. EFFECTS OF GAS ATTENUATION ON X-RAY PULSES

Let us try to quantify the pulse-to-pulse variations in the scattering response of the attenuator that may contribute to the ‘temporal’ incoherence from summing the pulses together. First, it is important to note that the attenuator is approximately 20 m upstream of the KB mirrors (see Fig. 1 in manuscript). Additionally, there are apertures on these KB mirrors, each about 1 mm in diameter, that permit photons that are inelastically and elastically scattered by the attenuator that are within 50 micro-radians from the optical axis.

Now, let us consider the variations in the number of nitrogen molecules illuminated by the XFEL pulses. At 14.36 torr (1914 Pa), an ideal non-interacting diatomic N_2 gas at $\sim 300\text{K}$ has a molecular density of 9.3×10^{23} molecules per m^3 . Let us further assume the XFEL pulse has a FWHM of at least 1 mm as it passes through the gas attenuator, which we resolve downstream to approximately 200×200 resolution elements. This means that an average of $\approx 10^{14} \pm 10^7$ nitrogen molecules are illuminated within each resolution element (i.e., $5\mu\text{m} \times 5\mu\text{m}$). In other words, the relative fluctuations in the number of illuminated molecules per resolution element is 10^{-7} .

Next, we estimate the effect these illuminated N_2 molecules have on the XFEL wavefront. For simplicity, we adopt a kinematic scattering approximation (ignoring multiple scattering). The exit wave of an x-ray plane wave (monochromatic approximation to the XFEL pulse) through the N_2 gas is phase shifted by

$$\exp[in_r 2\pi d/\lambda],$$

where n_r is the complex valued refractive index of N_2 (which depends on the gas density), d is the length of the illuminated N_2 gas along the optical axis, and λ is the x-ray photon’s wavelength. In this approximation, the intensity of the exit x-ray photons, relative to unscattered photons, is attenuated by

$$\exp[-\mu_a n t],$$

while the gas imparts an average coherent phase shift on the x-rays of

$$\exp[i\mu_e n t];$$

here we define $\mu_a = 2r_e\lambda f_2$ and $\mu_e = \mu_a f_1/(2f_2)$, r_e as the classical electron radius, the scattering factor of atomic Nitrogen $f = f_1 + if_2$, $n = 1.8 \times 10^{24}$ is the number density of scatterers (i.e., N atoms), and t is the physical path length of x-ray photons through the attenuator gas.

Given the N_2 gas attenuated the power of the incident x-rays by about 10^{-7} , we expect the incoming x-ray plane wave to have suffered an average elastically scattered phase shift

of $\approx 13 \times 2\pi$ (since the f_1/f_2 ratio of N is about 10). Combining the results from the last two sentences, we conclude that the attenuator mostly imparts a large but spatially uniform overall phase shift on the beam that exits from the attenuating gas, because the resolvable spatial variations in phase shift from elastic scattering is negligible.

The above calculation presumes that even though the N_2 gas absorbs most of the energy of the XFEL pulse, the gas can dissipate the heat efficiently to establish some kind of quasi-equilibrium when illuminated by a steady stream of 120 XFEL pulses per second (where this gas rapidly thermalizes with a heat reservoir held at 300K). The average molecular speed in this gas is about 700 ms^{-1} , which means that molecules about 10 times the FWHM away (10 mm) from the center of the XFEL beam can remix into the wake of an illuminated gas column within $20 \mu\text{s}$. This remixing time is far shorter than the 8 ms interval between pulses. Overall, given the total volume of gas in the attenuator, this implies that any number density fluctuations of the gas owing to a single XFEL pulse should have dissipated well before the next pulse arrives.

Should the effects of multiple scattering be added to this approximation, only the overall phase shift is expected to increase (i.e., the effective μ_e should increase). However, the relative fluctuations in scatterer density (n) between resolution elements should still be as small as before. Hence, we are again led to believe that the attenuator mostly imparts a spatially uniform overall phase shift on the exit wave.

If the aforementioned assumptions and approximations are valid, ultimately this means that we do not expect to detect any effects from the fluctuations in the number of illuminated particles in the attenuator at our resolution.

We should also note that the cross section for Compton scattering (one form of incoherent scattering) for Nitrogen, at this soft x-ray energy of 1.2 keV, is expected to be an order of magnitude lower than that of coherent elastic scattering. Nitrogen does not have any resonant scattering edges near this photon energy. Hence, the loss of coherent speckle contrast from a spray of incoherently scattered photons is not expected to be dominant. Nevertheless, we did not characterize the effects of other sources of incoherent scattering (e.g., Auger emission, etc). Hence, we must acknowledge that we have not fully ascertained the overall effects that such incoherent scattering had on our reconstructions.

REFERENCES

1. B. L. Henke, E. M. Gullikson, and J. C. Davis, "X-Ray interactions: Photoabsorption, scattering, transmission, and reflection at $E = 50\text{-}30,000 \text{ eV}$, $Z = 1\text{-}92$," *At. Data Nucl. Data Tables* **54**, 181–342 (1993).
2. D. D. Ryutov, R. M. Bionta, S. P. Hau-Riege, K. I. Kishiyama, D. McMahon, M. D. Roeben, S. Shen, and P. M. Stefan, "The physics of the gas attenuator for the linac coherent light source (LCLS)," *Tech. rep.*, Lawrence Livermore National Lab.(LLNL), Livermore, CA (United States) (2009).
3. A. Sanchez-Gonzalez, P. Micaelli, C. Olivier, T. R. Barillot, M. Ilchen, A. A. Lutman, A. Marinelli, T. Maxwell, A. Achner, M. Ag aker, N. Berrah, C. Bostedt, J. D. Bozek, J. Buck, P. H. Bucksbaum, S. C. Montero, B. Cooper, J. P. Cryan, M. Dong, R. Feifel, L. J. Frasinski, H. Fukuzawa, A. Galler, G. Hartmann, N. Hartmann, W. Helml, A. S. Johnson, A. Knie, A. O. Lindahl, J. Liu, K. Motomura, M. Mucke, C. O'Grady, J. E. Rubensson, E. R. Simpson, R. J. Squibb, C. S athe, K. Ueda, M. Vacher, D. J. Walke, V. Zhaunerchyk, R. N. Coffee, and J. P. Marangos, "Accurate prediction of x-ray pulse properties from a free-electron laser using machine learning," *Nat. Commun.* **8** (2017).